Supporting Information

X-ray crystallography–based structural elucidation of enzyme-bound intermediates along the 1-deoxy-D-xylulose 5-phosphate synthase reaction coordinate

Percival Yang-Ting Chen[‡], Alicia A. DeColli[§], Caren L. Freel Meyers[§,1], and Catherine L. Drennan[‡,¶,‖,1]

From the [‡]Department of Chemistry, Massachusetts Institute of Technology, Cambridge, MA 02139, USA; [§]Department of Pharmacology and Molecular Sciences, The Johns Hopkins University School of Medicine, Baltimore, MD 21205, USA; [¶]Department of Biology, Massachusetts Institute of Technology, Cambridge, MA 02139, USA; [‖]Howard Hughes Medical Institute, Massachusetts Institute of Technology, Cambridge, MA 02139, USA

[1]To whom correspondence should be addressed: Catherine L. Drennan, Department of Biology and Department of Chemistry, Massachusetts Institute of Technology, Cambridge, MA 02139, 31 Ames St, Building 68-680, Cambridge, MA 02139; cdrennan@mit.edu; Tel. (617) 253-5622; Fax. (617) 258-7847, and Caren L. Freel Meyers, Department of Pharmacology and Molecular Sciences, The Johns Hopkins University School of Medicine, Baltimore, MD 21205; cmeyers@jhmi.edu; Tel. (410) 502-4807; Fax. (410) 955-3023.

Table of Contents **Page**

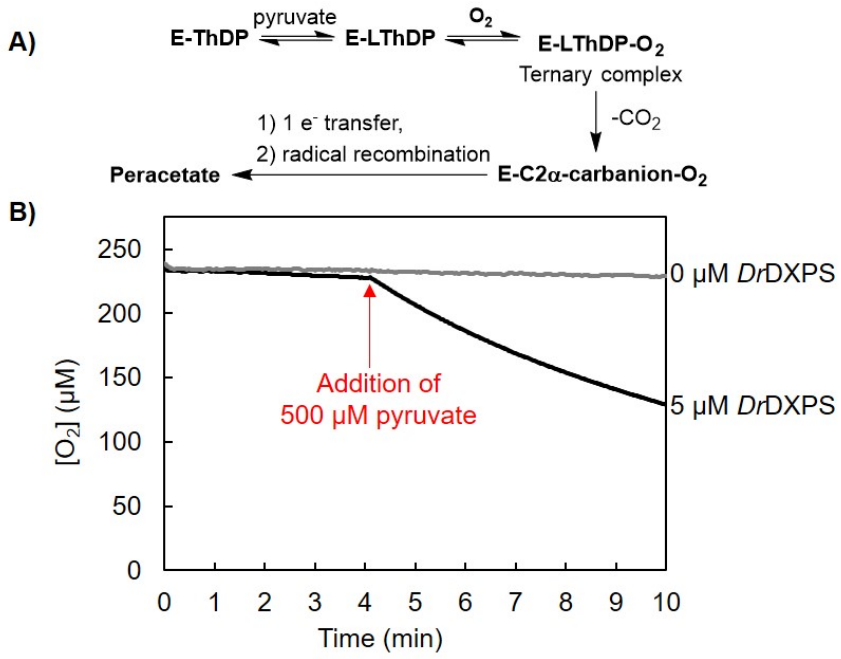

Figure S1. Oxygenase activity of DXPS. Oxygenase activity of *Dr*DXPS (A) was confirmed by monitoring enzyme-and pyruvate-dependent consumption of O_2 (B). In the presence of saturating pyruvate (500 μM) and *Dr*DXPS (5 μM) at 25 °C, O_2 depletion is observed (v = 20.7 ± 0.9 μM/min), indicating that O_2 contributes to pre-decarboxylation intermediate instability on *Dr*DXPS.

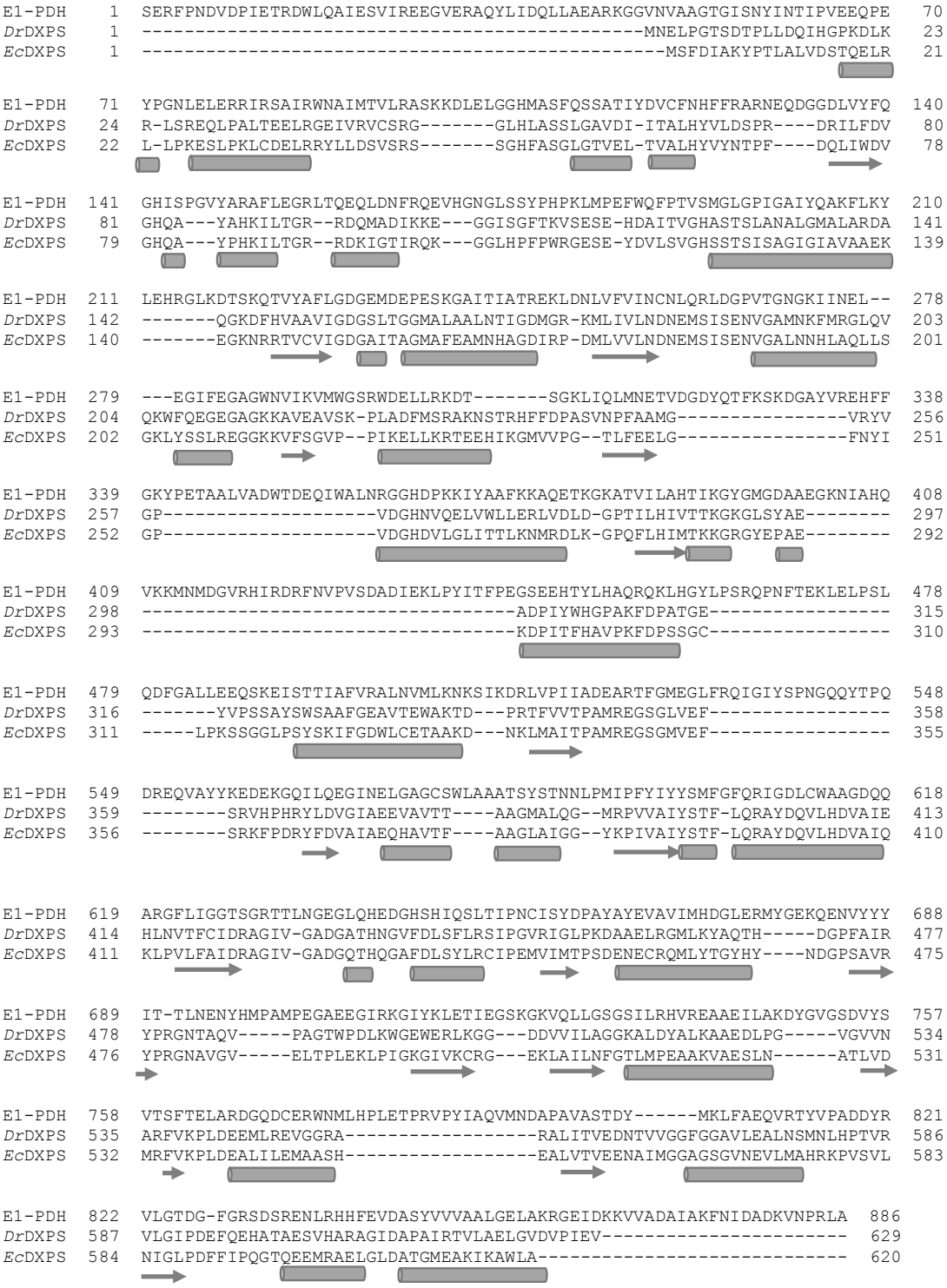

Figure S2. Sequence alignment of *Ec*DXPS (2O1S), *Dr*DXPS (2O1X), and E1-PDH (2G25). PROMALS3D (1) was used for the alignment. Secondary structure is indicated below the corresponding sequence where helix and beta sheet are denoted by a cylinder or arrow, respectively.

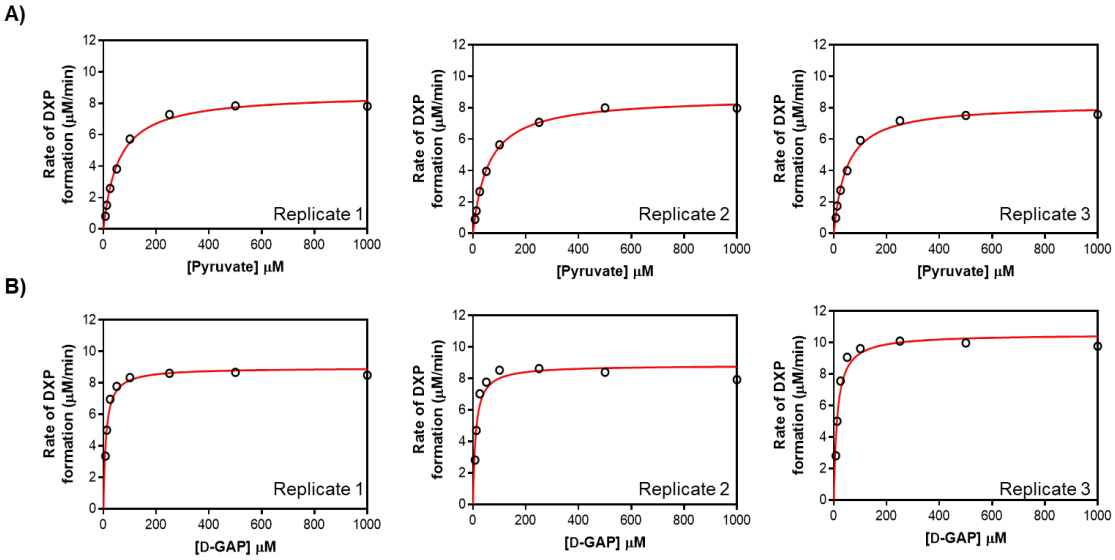

Figure S3. Michaelis-Menten kinetic analysis of *Dr*DXPS. Crystallization of *Dr*DXPS was conducted under anoxic conditions; thus, DXP-forming activity was confirmed under anoxic conditions. Michaelis-Menten analysis was conducted by varying pyruvate concentration (A) or varying D-GAP concentration (B). Similar to the kinetic parameters for other DXPS enzymes, $K_m^{pyruvate} = 54 \pm 3$ μM, $K_m^{D\text{-}GAP} = 11 \pm 2$ μM, and $k_{cat} = 45 \pm 2$ min^{-1} for *Dr*DXPS. Error represents standard error, $n = 3$ for K_m and $n = 6$ for k_{cat}.

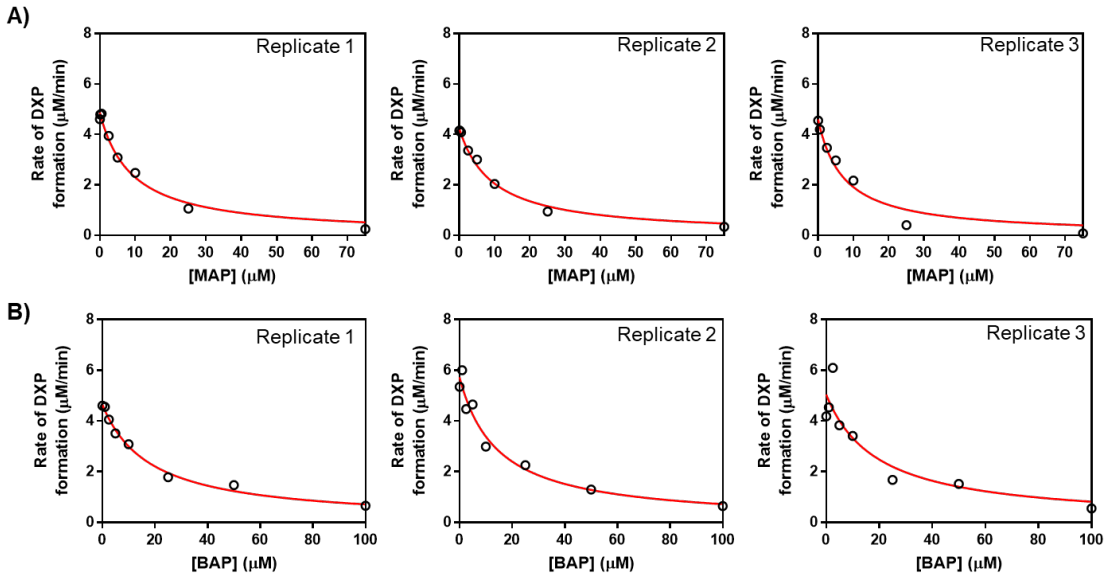

Figure S4. Morrison curves for (A) MAP and (B) BAP inhibition of DXP formation on *Dr*DXPS under anoxic conditions

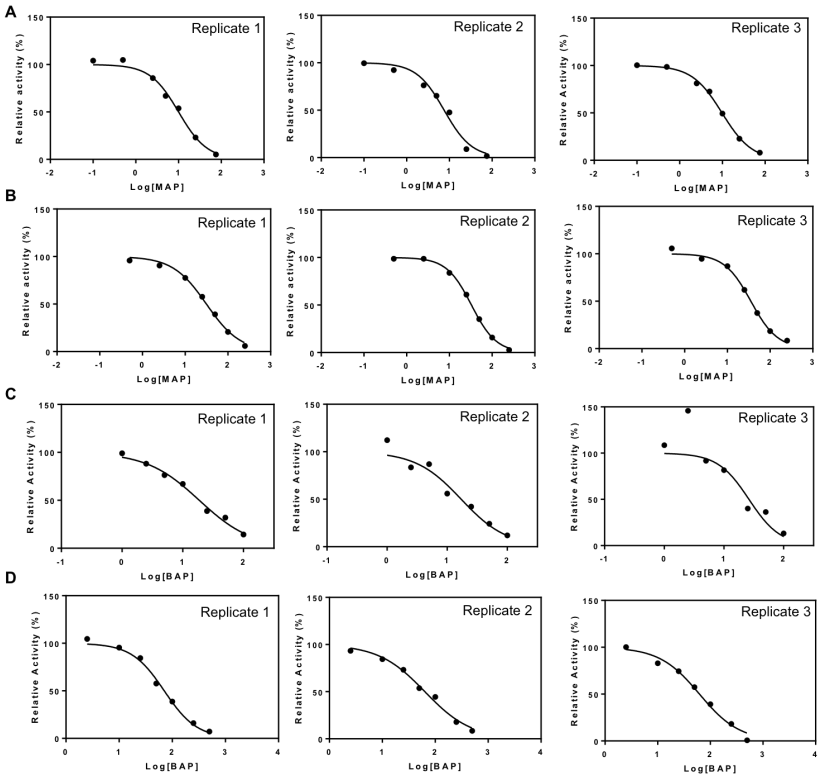

Figure S5. IC_{50} curves for (A-B) MAP and (C-D) BAP inhibition of DXP formation by *Dr*DXPS under anoxic conditions. Concentrations in μM were used for logarithm calculation. IC_{50} curves in panels (A) and (C) were conducted in the presence of $2\times K_m^{pyruvate}$, whereas curves in panel (B) and (D) were conducted in the presence of $10\times K_m^{pyruvate}$.

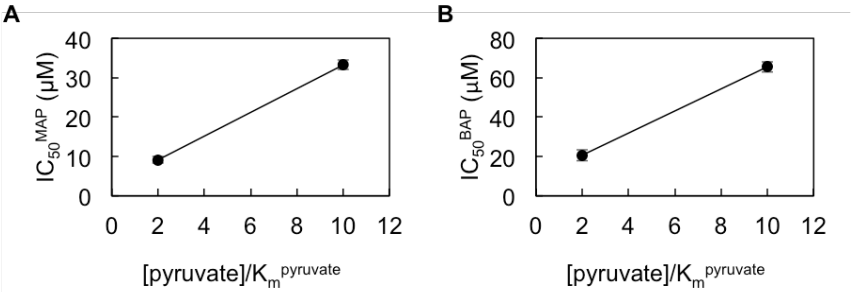

Figure S6. Determination of MOI of (A) MAP and (B) BAP against *Dr*DXPS. A positive slope indicates increasing IC_{50} with increasing [pyruvate] suggesting MAP and BAP are competitive with respect to pyruvate as expected. Error represents standard deviation, n = 3

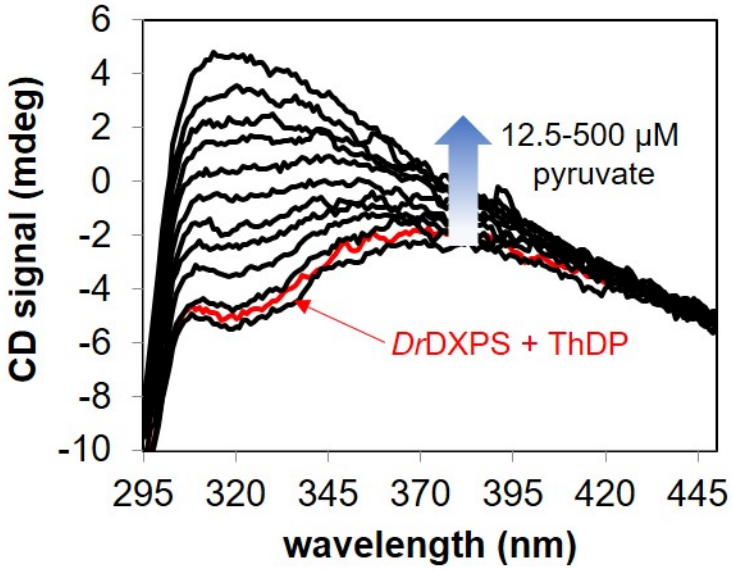

Figure S7. Accumulation of LThDP on *Dr*DXPS. The CD signal increases with the concentration of pyruvate (12.5, 25, 37.5, 50, 75, 100, 150, 200, 300, 400, and 500 µM), indicating the formation of the stable LThDP intermediate on *Dr*DXPS (50 µM).

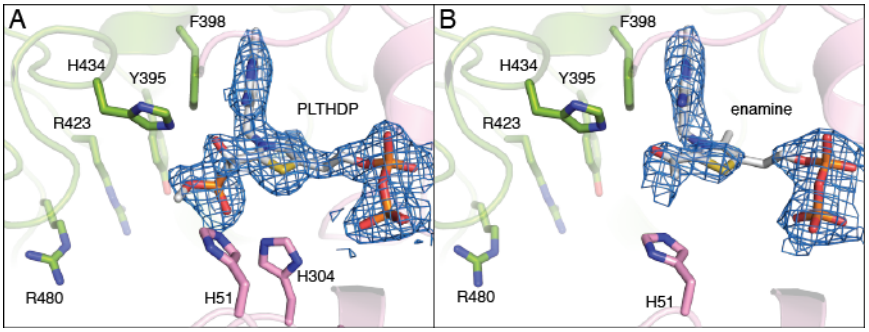

Figure S8. Composite omit electron density maps of ThDP-intermediate states captured in this study. (A) Composite omit map contoured to 1.0σ in blue mesh for PLThDP; (B) Composite omit map contoured to 1.0σ in blue mesh for the enamine. The structures are colored in the same color scheme as **Fig. 2.** Tyr395, Arg423 and Arg480, which have been implicated in D-GAP binding (2), are labeled.

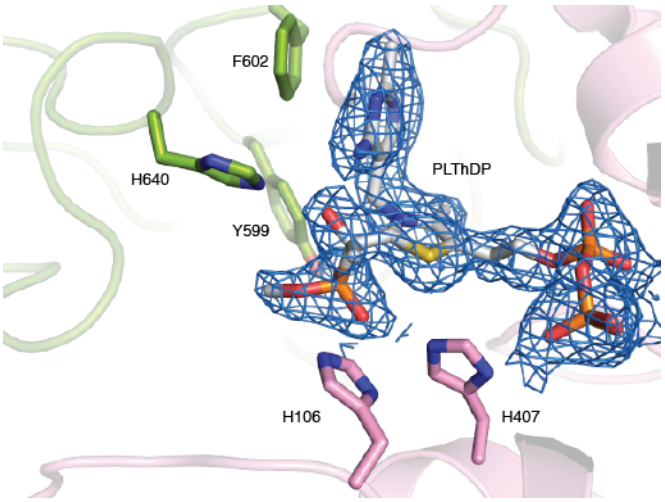

Figure S9. Composite omit electron density maps of PLThDP-bound E1-PDH (PDB ID: 2G25). (3) Composite omit map contoured to 1.0σ in blue mesh for PLThDP. The composite omit map was calculated using Phenix (4) with the dataset deposited on PDB. The structures are colored in the same color scheme as **Fig. 3B**. Key active site residues are labeled.

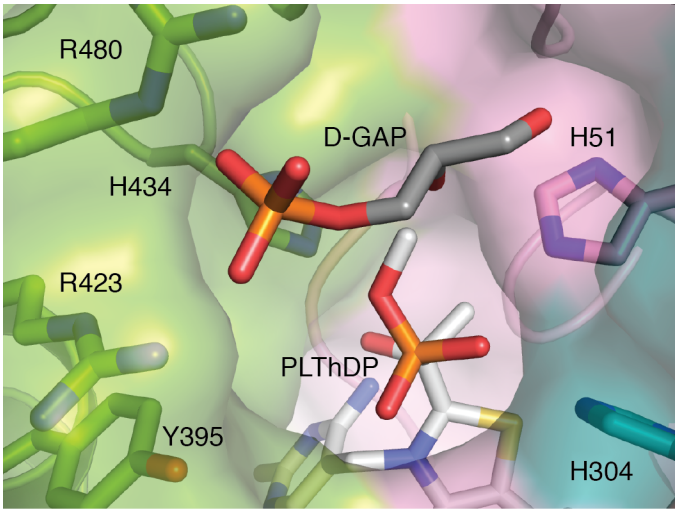

Figure S10. The active site of PLThDP-bound *Dr*DXPS with modeled D-GAP. The active site of *Dr*DXPS is large enough to bind PLThDP and D-GAP without clashes. The coordinates of D-GAP were reproduced from previous docking analysis (5). His51, His304, and His434, three predicted PLThDP-binding residues, are shown as sticks. Tyr395, Arg423 and Arg480, which have been implicated in D-GAP binding (2), are also shown as sticks.

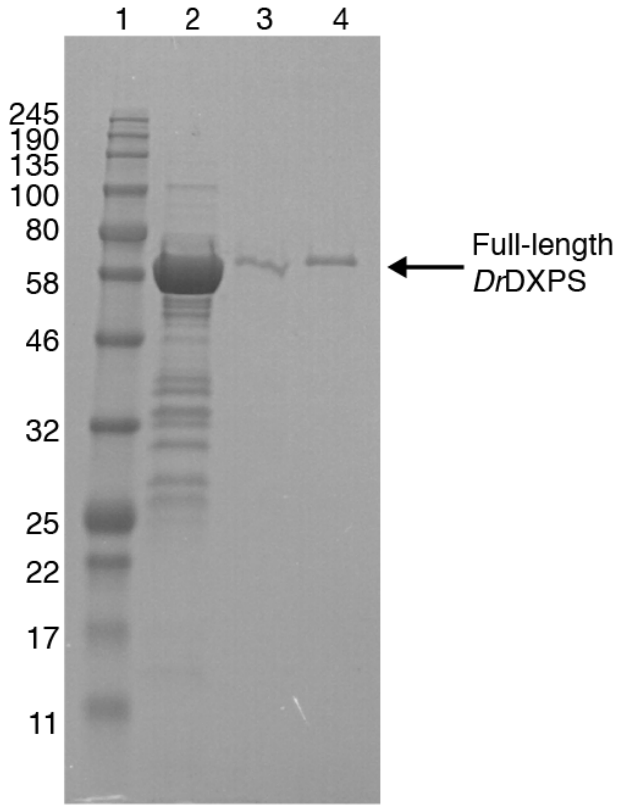

Figure S11. SDS-PAGE analysis of *Dr*DXPS cocrystallized with pyruvate. Lane 1, molecular weight markers (in kDa); Lanes 2, purified sample; Lane 3, crystallization drops; Lane 4, *Dr*DXPS crystals. *Dr*DXPS crystals were washed in 500 nL of well solution before harvested for SAS-PAGE analysis. *Dr*DXPS crystals show no sign of proteolysis.

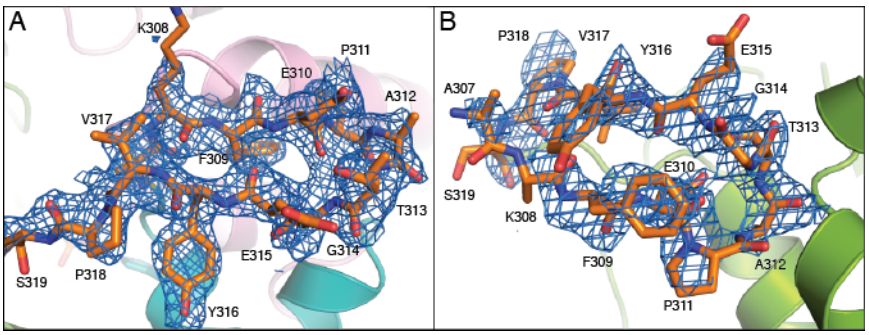

Figure S12. The composite omit electron density maps for the spoon motif in the structure of DXPS in the presence of (A) PLThDP and (B) the enamine. Composite omit maps are contoured to 1.0σ in blue meshes for the spoon motif. The continuous electron density validates the assigned conformations for the spoon motif in both structures. The structures are colored in the same color scheme as **Fig. 5A**.

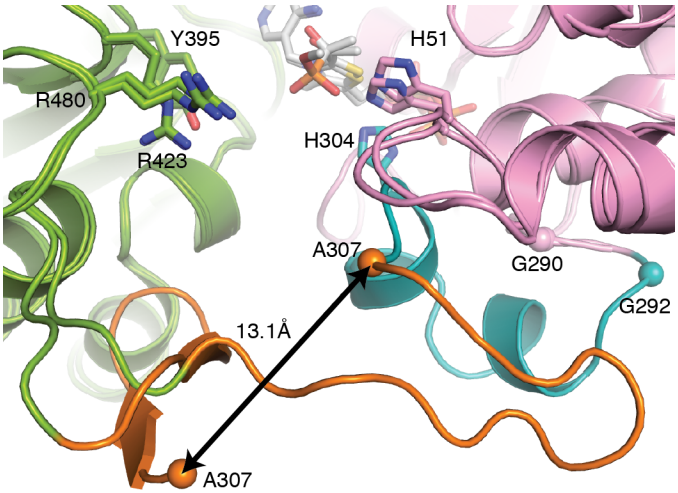

Figure S13. Active site rearrangements in *Dr*DXPS. The structure of *Dr*DXPS in the presence of PLThDP is overlaid with the structure of *Dr*DXPS cocrystallized with pyruvate. The spoon motif (orange) is shifted by 17 Å between two structures, and Ala307 is shifted by 13.1 Å. Tyr395, Arg423 and Arg480, which have been implicated in D-GAP binding (2), are labeled. Cαs of Gly290, Gly292, and Ala307 (if present in structures) are shown as spheres to highlight the conformational changes.

Table S1. Summary of kinetic parameters for DXP formation and inhibitory constants (K_i^{MAP} and K_i^{BAP}) for *Dr*DXPS and *Ec*DXPS (6,7) under anoxic conditions. Error represents standard error, n = 3 for K_m and K_i; n = 6 for k_{cat}.

Enzyme	$K_m^{D\text{-}GAP}$ (μM)	$K_m^{pyruvate}$(μM)	k_{cat}(min^{-1})	K_i^{MAP} (μM)	K_i^{BAP} (μM)
*Dr*DXPS	11 ± 2	54 ± 3	45 ± 2	2.8 ± 0.2	5.7 ± 0.5
*Ec*DXPS	6 ± 2[a]	20.77 ± 0.01[a]	92 ± 5[a]	3.24 ± 0.02[b]	5.6 ± 0.8[b]

[a]Data from DeColli, A. A., Nemeria, N. S., Majumdar, A., Gerfen, G. J., Jordan, F., and Freel Meyers, C. L. (2018) Oxidative decarboxylation of pyruvate by 1-deoxy-D-xyulose 5-phosphate synthase, a central metabolic enzyme in bacteria. *J. Biol. Chem.* **293**, 10857-10869

[b]Data from Smith, J. M., Vierling, R. J., and Freel Meyers, C. L. (2012) Selective inhibition of *E. coli* 1-deoxy-D-xylulose-5-phosphate synthase by acetylphosphonates. *MedChemComm* **3**, 65-67

Table S2. Data collection and model refinement statistics for structures of *Dr*DXPS.

	*Dr*DXPS with MAP bound	*Dr*DXPS with enamine bound
PDB ID	6OUV	6OUW
Beamline	APS 24-ID-C	APS 24-ID-C
Space group	$P2_12_12_1$	C2
Cell dimensions (Å)	a = 78.50, b = 125.28, c = 151.70	a = 129.75, b = 85.54, c = 60.57, β = 114.77^o
Wavelength (Å)	0.9791	0.9791
Resolution (Å) †	100-1.94 (2.01-1.94)	50.-2.40 (2.49-2.40)
# unique reflections	110177	23154
Completeness (%) †	98.6 (92.3)	98.2 (92.2)
Redundancy †	6.6 (5.7)	4.8 (2.9)
$\langle I/\sigma I \rangle$ †	22.4 (2.4)	7.8 (2.7)
R_{sym} †	0.076 (0.719)	0.139 (0.420)
$CC_{1/2}$ †	(0.806)	(0.833)
Resolution (Å)	96.6-1.94	49.4-2.40
# unique reflections	110075	23132
R_{work} (%) / R_{free} (%)	15.6/17.4	15.8/19.6
RMS bond lengths (Å)	0.003	0.003
RMS bond angles (^{o})	0.62	0.59
Number of Atoms/Molecules		
Protein atoms	8985	4093
PLThDP	2	0
enamine	0	1
Water molecules	607	114
Na^+	2	1
Average B-factor (Å^2)	44.8	54.4
Protein atoms	44.9	54.6
PLThDP	36.0	-
enamine	-	56.2
Water molecules	45.3	47.3
Na^+	33.5	52.7
Ramachandran plot		
Favored (%)	96.99	97.03
Allowed (%)	3.01	2.97
Outliers (%)	0.00	0.00
Rotamer outliers (%)	0.54	1.19

†Values in parentheses indicate the highest-resolution bin.

Table S3. Residues and cofactors modeled in each chain (1-629) of both structures.

	PLThDP-bound *Dr*DXPS	Enamine-bound *Dr*DXPS
A	8-208, 217-224, 244-629 1 PLThDP, 1 Na^+	7-185, 247-291, 307-626 1 enamine, 1 Na^+
B	8-200, 244-626 1 PLThDP, 1 Na^+	N/A

Table S4. Comparisons of model refinement statistics among the structure of *Dr*DXPS with MAP bound and two DXPS structures published before this work.

PDB ID	PLThDP-bound *Dr*DXPS 6OUV	*Dr*DXPS 2O1X (3)	Proteolyzed *Ec*DXPS 2O1S (3)
Resolution (Å)	96.60-1.94	29.25-2.90	29.77-2.40
Clash score	1.66	13	19
R_{work} (%) / R_{free} (%)	15.6/17.4	20.9/27.2	19.1/23.4
Ramachandran outliers (%)	0.00	1.7	0.4
Rotamer outliers (%)	0.54	9.7	4.3

References

1. Pei, J., and Grishin, N. V. (2014) PROMALS3D: multiple protein sequence alignment enhanced with evolutionary and three-dimensional structural information. *Methods Mol. Biol.*, 263-271
2. Basta, L. A. B., Patel, H., Kakalis, L., Jordan, F., and Freel Meyers, C. L. (2014) Defining critical residues for substrate binding to 1-deoxy-D-xylulose 5-phosphate synthase – active site substitutions stabilize the predecarboxylation intermediate C2α-lactylthiamin diphosphate. *FEBS J.* **281**, 2820-2837
3. Xiang, S., Usunow, G., Lange, G., Busch, M., and Tong, L. (2007) Crystal structure of 1-deoxy-D-xylulose 5-phosphate synthase, a crucial enzyme for isoprenoids biosynthesis. *J. Biol. Chem.* **282**, 2676-2682
4. Adams, P. D., Afonine, P. V., Bunkóczi, G., Chen, V. B., Davis, I. W., Echols, N., Headd, J. J., Hung, L.-W., Kapral, G. J., and Grosse-Kunstleve, R. W. (2010) PHENIX: a comprehensive Python-based system for macromolecular structure solution. *Acta Crystallogr. D Biol. Crystallogr.* **66**, 213-221
5. Brammer, L. A., Smith, J. M., Wade, H., and Freel Meyers, C. L. (2011) 1-Deoxy-D-xylulose 5-phosphate synthase catalyzes a novel random sequential mechanism. *J. Biol. Chem.* **286**, 36522-36531
6. Smith, J. M., Vierling, R. J., and Freel Meyers, C. L. (2012) Selective inhibition of *E. coli* 1-deoxy-D-xylulose-5-phosphate synthase by acetylphosphonates. *MedChemComm* **3**, 65-67
7. DeColli, A. A., Nemeria, N. S., Majumdar, A., Gerfen, G. J., Jordan, F., and Freel Meyers, C. L. (2018) Oxidative decarboxylation of pyruvate by 1-deoxy-D-xyulose 5-phosphate synthase, a central metabolic enzyme in bacteria. *J. Biol. Chem.* **293**, 10857-10869